Nuclear Instruments and Methods in Physics Research A 763 (2014) 502–509

Contents lists available at ScienceDirect

Nuclear Instruments and Methods in Physics Research A

journal homepage: www.elsevier.com/locate/nima

Sensitivity booster for DOI-PET scanner by utilizing Compton scattering events between detector blocks

Eiji Yoshida *, Hideaki Tashima, Taiga Yamaya

Molecular Imaging Center, National Institute of Radiological Sciences, 4-9-1 Anagawa, Inage-ku, Chiba 263-8555, Japan

ARTICLE INFO

Article history:
Received 11 April 2014
Received in revised form
13 June 2014
Accepted 1 July 2014
Available online 10 July 2014

Keywords:
PET
Sensitivity
Compton scatter
Simulation

ABSTRACT

In a conventional PET scanner, coincidence events are measured with a limited energy window for detection of photoelectric events in order to reject Compton scatter events that occur in a patient, but Compton scatter events caused in detector crystals are also rejected. Scatter events within the patient causes scatter coincidences, but inter crystal scattering (ICS) events have useful information for determining an activity distribution. Some researchers have reported the feasibility of PET scanners based on a Compton camera for tracing ICS into the detector. However, these scanners require expensive semiconductor detectors for high-energy resolution. In the Anger-type block detector, single photons interacting with multiple detectors can be obtained for each interacting position and complete information can be gotten just as for photoelectric events in the single detector. ICS events in the single detector have been used to get coincidence, but single photons interacting with multiple detectors have not been used to get coincidence. In this work, we evaluated effect of sensitivity improvement using Compton kinetics in several types of DOI-PET scanners. The proposed method promises to improve the sensitivity using coincidence events of single photons interacting with multiple detectors, which are identified as the first interaction (FI). FI estimation accuracy can be improved to determine FI validity from the correlation between Compton scatter angles calculated on the coincidence line-of-response. We simulated an animal PET scanner consisting of 42 detectors. Each detector block consists of three types of scintillator crystals (LSO, GSO and GAGG). After the simulation, coincidence events are added as information for several depth-of-interaction (DOI) resolutions. From the simulation results, we concluded the proposed method promises to improve the sensitivity considerably when effective atomic number of a scintillator is low. Also, we showed that FI estimate accuracy is improved, as DOI resolution is high.

1. Introduction

In a conventional PET scanner, coincidence events are measured with a limited energy window for detection of photoelectric events to reject Compton scatter events that occur in a patient, but Compton scatter events caused in detector crystals are also rejected. Scatter events within the patient cause scatter coincidences, but inter crystal scattering (ICS) events have useful information for determining an activity distribution. Some researchers [1–4] have reported feasibility of PET scanners based on a Compton camera for tracing ICS into the detector. We have proposed a random reduction method of the ICS events for a scintillation-based depth-of-interaction (DOI) detector [5] with independent signal output that learned the correlation between irradiation angle and distribution of signal outputs [3]. However, it is difficult to trace the ICS into the detector for a conventional Anger-type block detector. Also, Chinn et al. [4] have proposed a random rejection method using the difference between Compton scatter angles calculated from deposited energy and coincidence line-of-response (LOR) using a semiconductor detector. Tracing the gamma ray behavior, however, requires an expensive semiconductor detector for high-energy resolution.

In the Anger-type block detector, single photons interacting with multiple detectors can be obtained for each interacting position and complete information can be gotten just as for photoelectric events in the single detector. ICS events in the single detector have been used to get coincidence, but single photons interacting with multiple detectors have not been used to get coincidence. Some researchers [6–10] have reported first interaction estimation methods of ICS using information of DOI, energy and time-of-flight for improving spatial resolution and sensitivity. We have developed the 4-layer DOI detector [5] and X'tal cube detector with 1-mm isotropic resolution [11,12]. The detectors

* Corresponding author. Tel.: +81 43 206 3260; fax: +81 43 252 7380.
E-mail address: rush@nirs.go.jp (E. Yoshida).

http://dx.doi.org/10.1016/j.nima.2014.07.002
0168-9002/

with high DOI resolution can trace the gamma ray behavior more precisely compared to a conventional PET detector. In this work, we evaluated effect of sensitivity improvement using Compton kinetics in several types of scintillator-based DOI-PET scanners.

2. Materials and methods

2.1. Identification of the first interaction among event interacting with multiple detectors

Fig. 1 illustrates a single photon interacting with multiple detectors in a coincidence event. Conventionally, these events are not only limited by the energy window, and they also cannot be identified by the interaction sequence as shown in Fig. 2. Our proposed method promises to improve the sensitivity using this event, which is identified as the first interaction (FI). Fig. 3 shows a flow chart of FI identification for the proposed method. The proposed method requires single data and applies coincidence detection by software. First, the proposed method applied the coincidence time window before the energy window for obtained events interacting with multiple detectors. Also, events interacting with multiple detectors are limited by a closely-aligned detector in the axial and transaxial directions. Compton interactions tend to be forward scattering and DOI and energy information may provide a way to identify the FI. If the detected coincidence event is interacting with multiple detectors, we apply preprocessing for the FI judgment rule as follows:

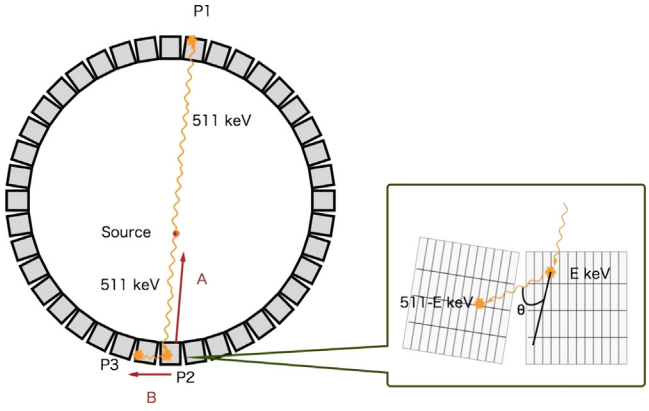

Fig. 1. Illustration of a single photon interacting with multiple detectors in a coincidence event.

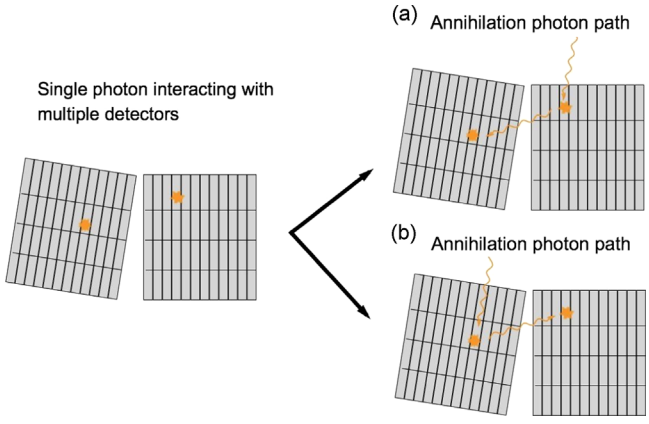

Fig. 2. Illustration of annihilation photon paths for the single photon interacting with multiple detectors.

- If the layers interacting with multiple detectors are different, the detector interacting with the upper layer has the FI.
- If the layers interacting with multiple detectors are the same, the detector interacting with higher deposited energy has the FI.

However, FI estimation of this preprocessing is not accurate. In the proposed method, FI estimation accuracy can be improved to determine validity of the FI from the correlation between Compton scatter angles calculated from deposited energy and coincidence LOR. Compton scatter angle of irradiation radiation θ can be defined by the two equations as follows:

$$\theta_{energy} = \cos^{-1}\left(\frac{2E-511}{E-511}\right)$$

$$\theta_{LOR} = 180 - \cos^{-1}\left(\frac{A \times B}{|A||B|}\right) \quad (1)$$

where, A and B are vectors based on the origin of the FI position as shown in Fig. 1. Angle resolutions of θ_{Energy} and θ_{LOR} naturally depend on detector performance. In the preprocessing part,

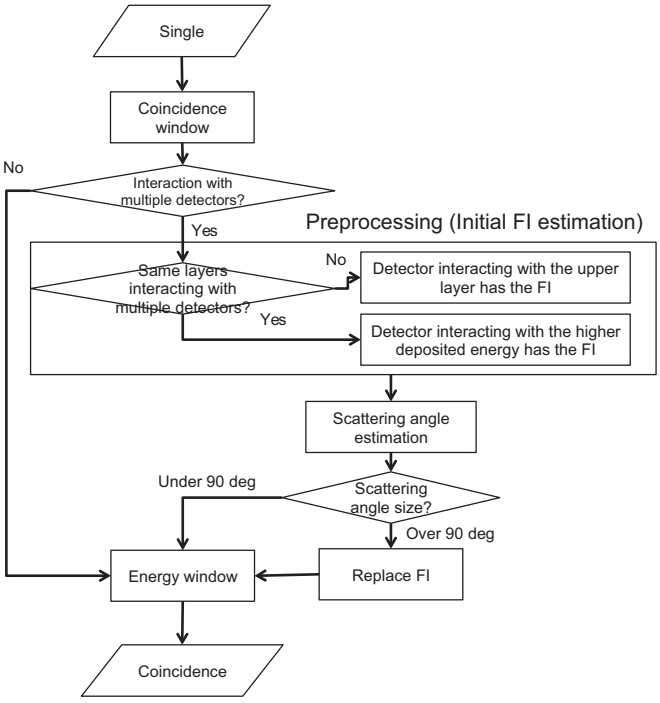

Fig. 3. Flow chart of FI identification for proposed method.

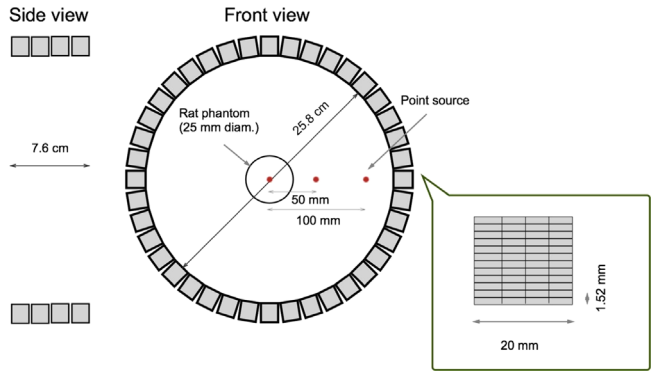

Fig. 4. Simulation setup. In this case, the DOI resolution was 5 mm.

Compton interaction is assumed to be forward scattering. Therefore, events with large Compton scatter angle cause a false FI estimation. The threshold of the false FI estimation is 90 deg.

Fig. 5. Illustration of the error distance between interacted crystals for the single photon interacting with multiple detectors.

We considered a small animal DOI-PET scanner, because the number of events interacting with multiple detectors is increased, as size of the detector block is smaller. Also, the number of events interacting with multiple detectors depends strongly on effective of the scintillator. We evaluated performance of the proposed method using several kinds of scintillator.

2.2. Monte-Carlo simulation

We evaluated performance characteristics of the DOI-PET scanner applying the proposed method using the Geant4 application for tomographic emission (GATE) [13,14] simulation. GATE has been used for simulating several PET scanners and reliability and usefulness of the GATE platform have been validated. The simulated animal PET scanner, based on the microPET Focus 220, consisted of 42 detectors arranged in four rings with a ring diameter of 25.8 cm as shown in Fig. 4. Each detector block consisted of a 12×12 array of three types of scintillator crystals (LSO, GSO and GAGG [15,16]). The dimensions of each scintillator crystal were $1.52\ \text{mm} \times 1.52\ \text{mm} \times 20\ \text{mm}$. From the microPET configuration, the crystal length was extended from 10 mm to 20 mm. Also, the DOI-PET scanner was assumed to have single photon-based data acquisition and software-based coincidence detection. Single data was obtained using the energy window of 50–650 keV. After the simulation, coincidence events were added as information at several DOI resolutions (from 1.25 mm to 10 mm). This simple crystal identification indicates ideal interacting crystals without any crystal decoding error. On the other hand, ICS also causes miss-positioning of interaction points. The identified crystal

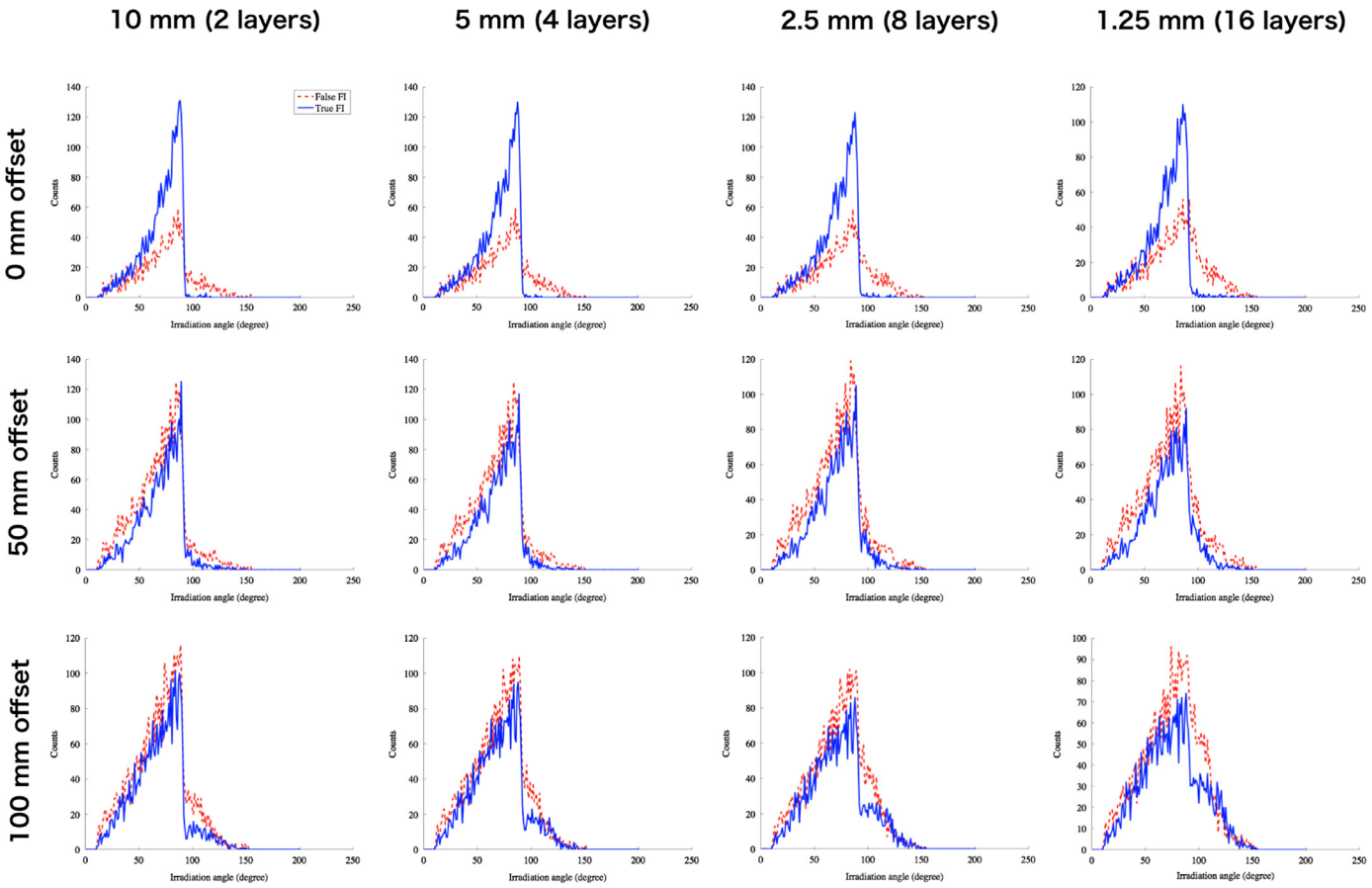

Fig. 6. Distributions of Compton scatter angles of the LSO crystals calculated from energy information with several DOI resolutions and several source positions for the point source. The solid line shows events with true FI estimation and the dashed line show events with false FI estimation.

is determined by finding the centroid. This is essentially the scheme being used in a conventional PET detector.

For evaluation of the proposed method, we simulated a point source at several offset position. Also, we calculated sensitivity and noise equivalent count rate (NECR) for a cylinder phantom (150 mm long, 50 mm diameter). This phantom was filled with ^{18}F water and was placed in the center of the FOV. Energy windows of LSO, GSO and GAGG crystals were 400–650 keV, 400–650 keV and 450–650 keV, respectively. Coincidence time windows of LSO, GSO and GAGG crystals were 4.5 ns, 10 ns and 10 ns, respectively. The NECR was calculated as follows:

$$\mathrm{NECR} = \frac{T^2}{T+S+R} \tag{2}$$

where, T, S and R are the true, scatter, and random count rates, respectively.

2.3. Correct answer rate and error distance

To evaluate the FI estimation accuracy, we defined a correct answer rate and an error distance as figures of merit for the proposed method. First, each correct interaction sequence was obtained for the events interacting with multiple detectors. Then, FI of each event interacting with multiple detectors was identified using the proposed method. The correct answer rate, which represents the probability of correct crystal identification, was defined as:

$$\text{Correct answer rate} = \frac{\text{Number of multiple events whose FI estimation was correct}}{\text{Number of incident multiple events}}. \tag{3}$$

Fig. 5 illustrates the error distance between interacted crystals for the single photon interacting with multiple detectors. The error distance was defined as the distance between the center position of the second interaction crystal and the LOR. This error distance evaluated only the error of a single photon interacting with multiple detectors. Therefore, when the FI estimation was right, the error distance was zero.

3. Results

3.1. Point source

Fig. 6 shows distributions of Compton scatter angles of the LSO crystals calculated from energy information with several DOI resolutions and several source positions for the point source. Energy information did not supported identification the FI. On the other hand, Fig. 7 shows distributions of Compton scatter angles of the LSO crystals calculated from coincidence LOR information with several DOI resolutions and several source positions for the point source. At 0 mm offset, events with true FI estimation were distributed at angles less than about 100 deg. On the other hand, events with false FI estimation were distributed at angles above about 80 deg. Peaks at around 90 deg were events in which the layers interacting with multiple detectors were the same and FI of these events could not be identified. Also, as the DOI resolution was improved, the FI estimation accuracy was improved. This peak decreased as the source position was moved farther from the center. Therefore, if the true FIs are distributed to an area that is less than 90 deg, the estimated FIs are judged to be right. In the remaining area, the second interacting detector judged the FIs.

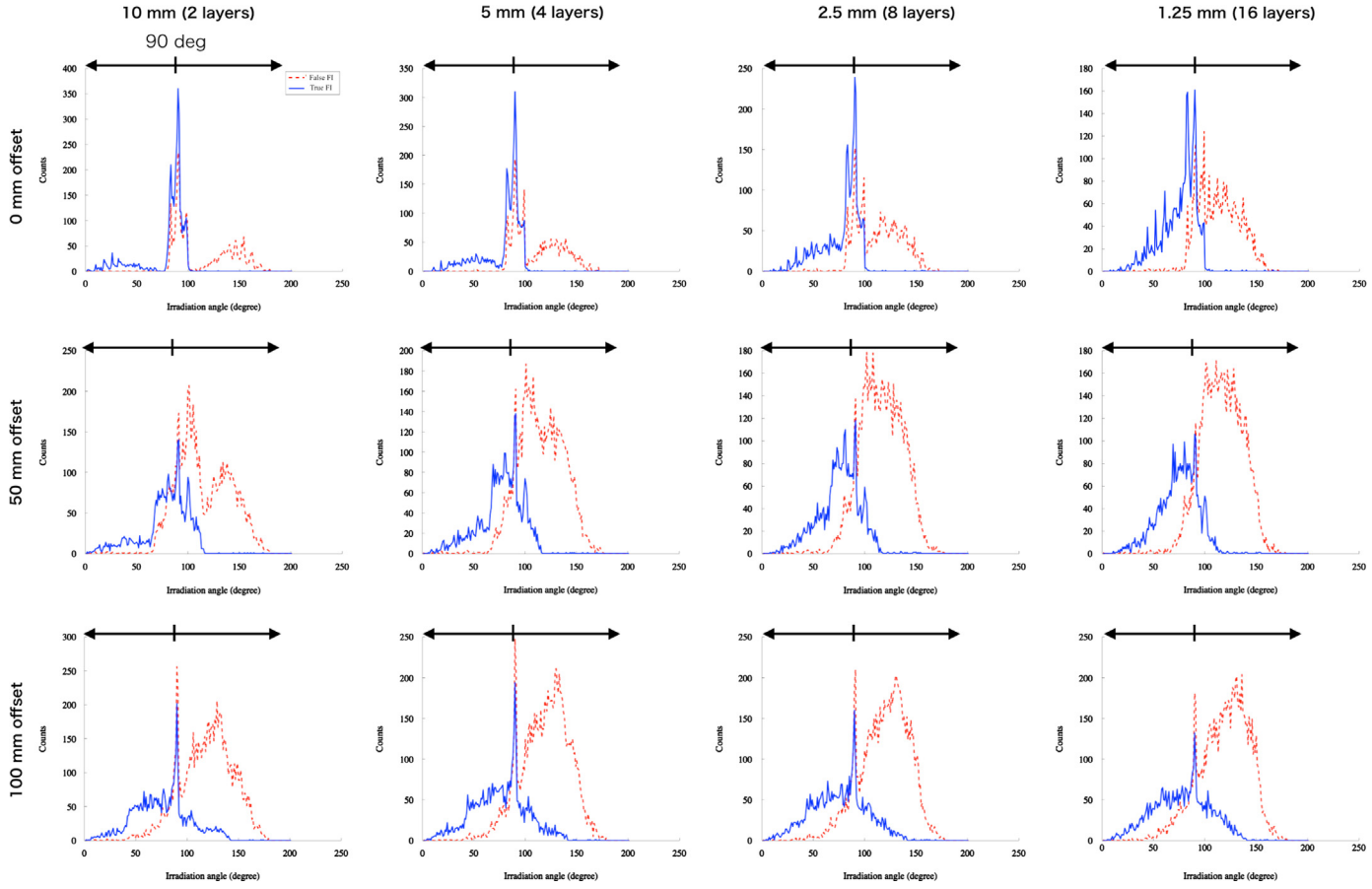

Fig. 7. Distributions of Compton scatter angles of the LSO crystals calculated from coincidence LOR information with several DOI resolutions and several source positions for the point source. The solid line shows events with true FI estimation and the dashed line shows events with false FI estimation.

Table 1 shows the correct answer rate of FI estimation of the LSO crystals for several source positions using the proposed method. The correct answer rate for only preprocessing was less than 50%. As the source offset position became farther from the center of the FOV, the correct answer rate of only preprocessing decreased. On the other hand, using the proposed method, the correct answer rate improved to 70–80% for 10-mm DOI resolution. Also, as the DOI resolution was improved, the correct answer rate was improved.

Fig. 8 shows error distance distributions of only false FI estimations for the point source with several DOI resolutions at 0 mm offset position for the LSO crystals. Total count of the false FI estimation of the 10 mm DOI resolution could be reduced significantly using the proposed method. As the DOI resolution was improved, the number of false FI estimations became smaller. Table 2 shows mean error distances of FI events of the LSO crystals for several source positions obtained using the proposed method. As the DOI resolution was improved, the mean error distance became smaller.

3.2. Cylinder phantom

Fig. 9 shows distributions of Compton scatter angles calculated from coincidence LOR information with several DOI resolutions

Table 2
Mean error distances of FI events of the LSO crystals for several source positions using the proposed method.

Offset position (mm)	Mean error distance (mm)				
	Only preprocessing	Proposed method			
	10 mm (2 Layers)	10 mm (2 Layers)	5.0 mm (4 Layers)	2.5 mm (8 Layers)	1.25 mm (16 Layers)
0	2.0	1.2	0.9	0.7	0.5
50	4.3	1.2	0.8	0.7	0.7
100	5.2	1.0	1.0	1.2	1.4

Table 1
Correct answer rate of FI estimation of the LSO crystals for several source positions using the proposed method.

Offset position (mm)	Correct answer rate of FI estimation (%)				
	Only preprocessing	Proposed method			
	10 mm (2 Layers)	10 mm (2 Layers)	5.0 mm (4 Layers)	2.5 mm (8 Layers)	1.25 mm (16 Layers)
0	50.8	71.6	75.5	80.8	86.7
50	30.5	77.8	83.5	86.7	87.9
100	29.8	81.2	82.2	81.9	80.6

Table 3
Correct answer rate of FI estimation for the cylinder phantom using the proposed method.

Scintillator	Correct answer rate of FI estimation (%)				
	Only preprocessing	Proposed method			
	10 mm (2 Layers)	10 mm (2 Layers)	5.0 mm (4 Layers)	2.5 mm (8 Layers)	1.25 mm (16 Layers)
LSO	34.6	72.8	78.5	83.1	87.2
GSO	39.6	73.1	80.1	84.8	88.2
GAGG	42.4	71.8	79.8	84.8	86.9

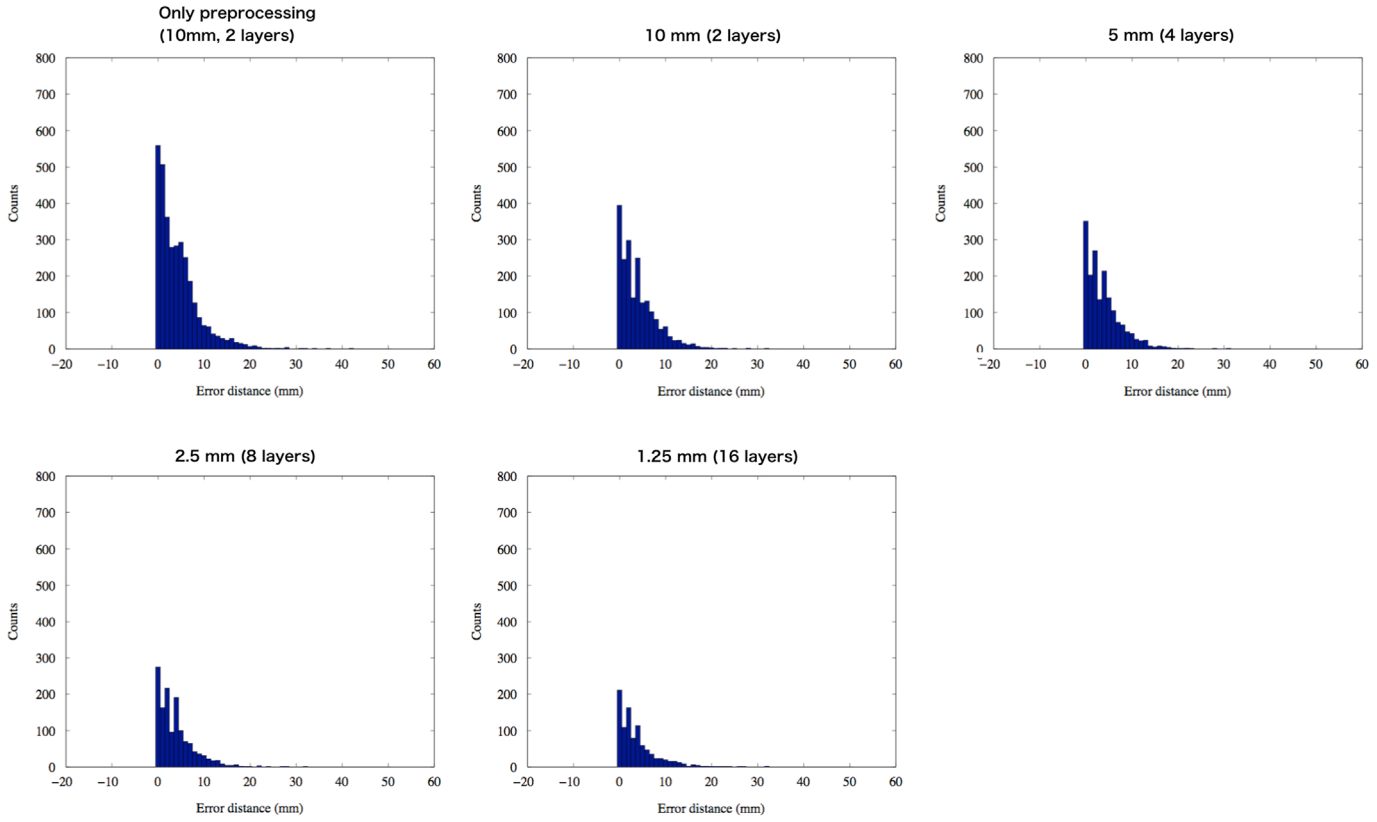

Fig. 8. Error distance distribution of only false FI estimation for the point source with several DOI resolutions at 0 mm offset position for the LSO crystals.

and several types of scintillator crystals for the cylinder phantom. Also, Table 3 shows the correct answer rate of FI estimation for the cylinder phantom using the proposed method. The correct answer rate using only preprocessing decreased, as the effective atomic number of the scintillators was high. On the other hand, we observed no difference among types of scintillator using the proposed method. As the DOI resolution was improved, performance of FI estimation was improved as well as the point source results.

Fig. 10 shows the error distance distribution of only false FI estimations with several DOI resolutions for the LSO crystals and the cylinder phantom. Table 4 shows mean error distances of FI events for the cylinder phantom obtained using the proposed method. As the effective atomic number of the scintillator was lower, the mean error distance was larger.

Table 5 shows sensitivities for several detector configurations using the proposed method. Sensitivities could be improved for all detector configurations by using single photons interacting with multiple detectors. Especially, the proposed method was efficient when the effective atomic number of the scintillator was low.

Table 4
Mean error distances of FI events for the cylinder phantom using the proposed method.

Scintillator	Mean error distance (mm)				
	Only preprocessing	Proposed method			
	10 mm (2 Layers)	10 mm (2 Layers)	5.0 mm (4 Layers)	2.5 mm (8 Layers)	1.25 mm (16 Layers)
LSO	3.5	1.3	0.9	0.7	0.6
GSO	3.5	1.6	1.1	0.9	0.7
GAGG	3.5	1.7	1.1	0.9	0.8

Table 5
Sensitivities for several detector configurations using the proposed method.

Scintillator	Sensitivity (%)		Gain (%)
	Conventional	Proposed method	
LSO	1.28	1.66	29.3
GSO	0.77	1.14	48.7
GAGG	0.62	1.01	62.6

3.3. NECR

Fig. 11 shows NECR curves with the three types of scintillator using the proposed method for the cylinder phantom. NECRs with LSO, GSO and GAGG crystals at the 400 MBq were improved by about 27%, 40% and 50%, respectively. In this case, random and scatter coincidences were increased as well as the true coincidence. However, the proposed method showed sufficient improvement of the NECR.

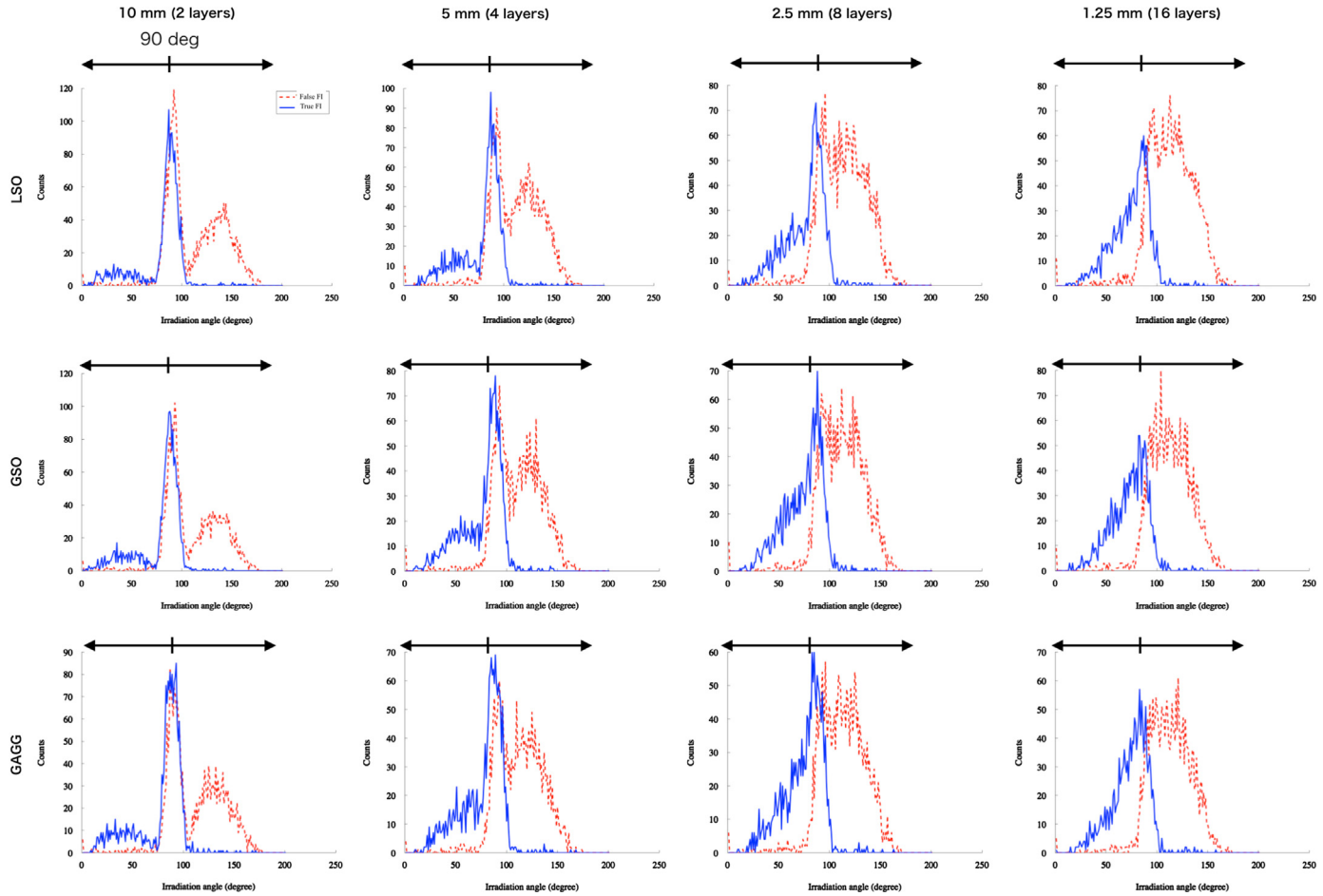

Fig. 9. Distributions of Compton scatter angles calculated from coincidence LOR information with several DOI resolutions and several types of scintillator crystals for the cylinder phantom. The solid line shows events with true FI estimation and the dashed line shows events with false FI estimation.

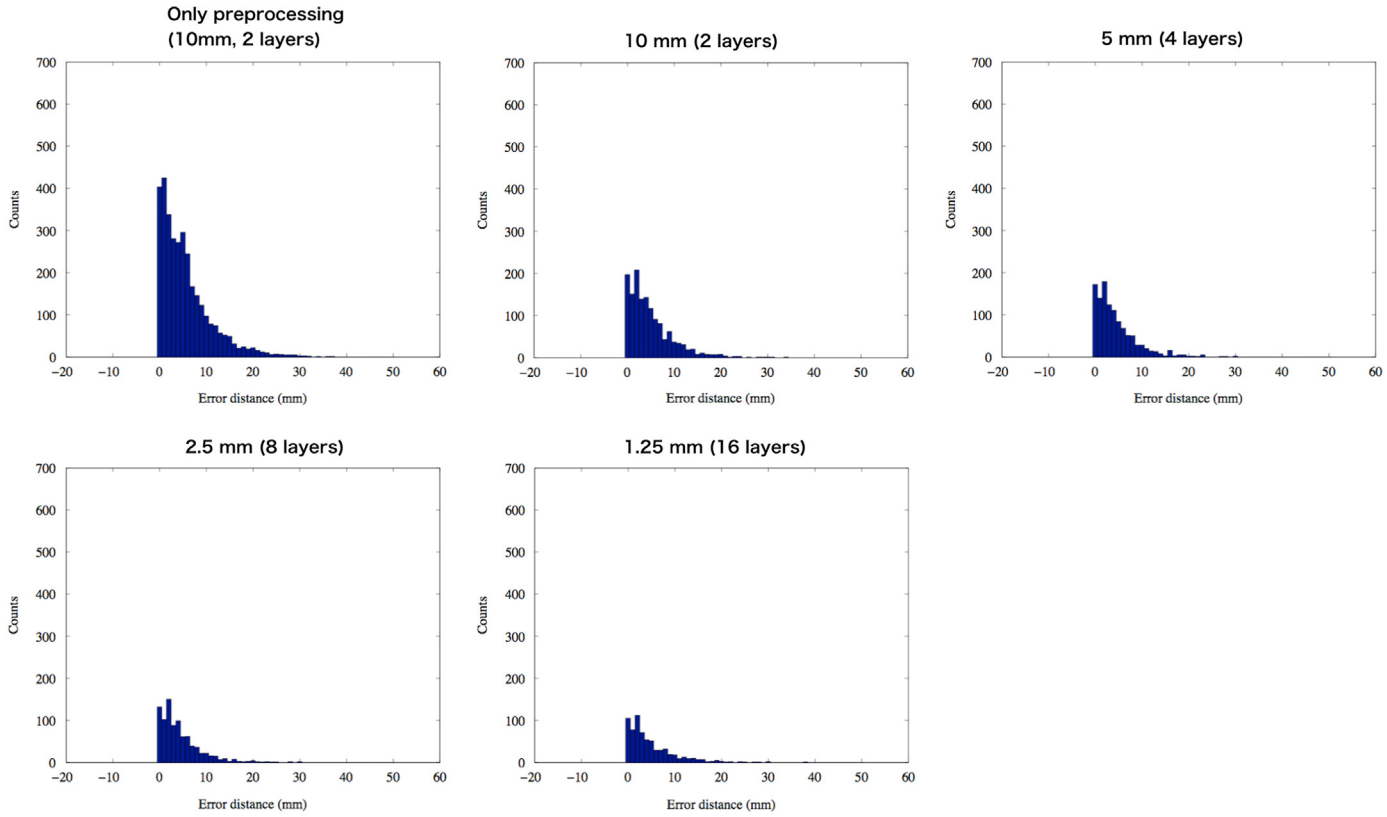

Fig. 10. Error distance distribution of only false FI estimation with several DOI resolutions for the LSO crystals and the cylinder phantom.

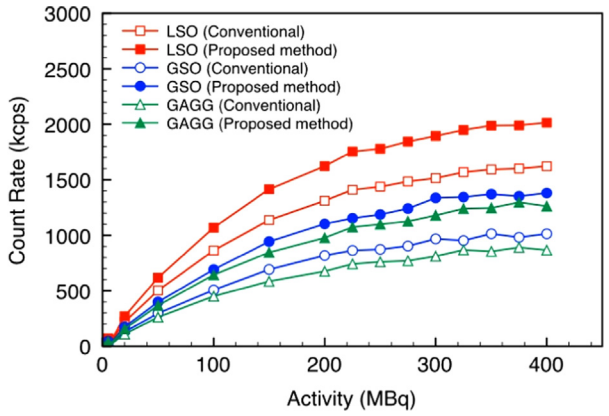

Fig. 11. NECR curves with several detector configurations using the proposed method for the cylinder phantom.

4. Discussion and conclusions

In this work, we evaluated effect of sensitivity improvement using Compton kinetics in several types of scintillator-based DOI-PET scanners. Using the coincidence LOR information, our proposed method promises to improve the sensitivity considerably while maintaining spatial resolution, when effective atomic number of a scintillator is low. Also, we showed that FI estimation accuracy was improved, as DOI resolution was higher. On the other hand, the energy information did not support identification of the FI. This is because the energy resolution of the scintillator detector is poor compared to that of a semiconductor detector.

The number of events interacting with multiple detectors depends strongly on effective atomic number of the scintillator. The effective atomic numbers of GSO and GAGG crystals are lower than that of LSO crystal. However, these scintillators have other merits compared to the LSO crystal. For example, the GAGG crystal has higher energy resolution than that of LSO crystal. Also, GSO and GAGG crystals are scintillators without intrinsic radioactivity. Therefore, the proposed method can compensate for the lower sensitivity of these scintillators.

In general, DOI information can minimize the effect of the crystal penetration of obliquely incident gamma rays. Then, the DOI-PET scanner can position detector rings closer to a patient for higher sensitivity. The proposed method is expected to improve sensitivity further using events interacting with multiple detectors. However, for accurate FI estimation, the detector must have high DOI resolution. Currently, many researchers continue to develop DOI detectors to achieve higher DOI resolution. Our X'tal cube detector also promises high FI estimation to achieve isotropic 3D positioning detectability.

The DOI-PET scanner designs have a larger occupancy of the FOV relative to the detector ring than a conventional PET scanner because the DOI-PET scanner designs allow a larger irradiation angle into the detector. As the radioactive source is set farther from the center of the FOV, the number of events interacting with multiple detectors is increased. Also, the event with a large irradiation angle is favored over events interacting with multiple detectors even when the Compton scatter angle is small. This means the assumed prepossessing of the FI judgment rule is incorrect as shown in Table 1. The proposed method improved the FI estimation accuracy for evaluation of the Compton scatter angle.

Acknowledgment

This work was supported by a Grant-in-Aid for Scientific Research (No. 24601019) from the Japan Society for the Promotion of Science.

References

[1] S.-J. Park, W.L. Rogers, N.H. Clinthorne, IEEE Trans. Nucl. Sci. NS54 (2007) 1543.
[2] S.-J. Park, W.L. Rogers, S. Huh, H. Kagan, K. Honscheid, D. Burdette, E. Chesi, C. Lacasta, G. Llosa, M. Mikuz, A. Studen, P. Weilhammer, N.H. Clinthorne, Phys. Med. Biol. 52 (2007) 2807.
[3] E. Yoshida, Y. Kimura, K. Kitamura, F. Nishikido, T. Yamaya, H. Murayama, IEEE NSS-MIC 2005 (2005) 1800.
[4] G. Chinn, C.S. Levin, IEEE NSS-MIC 2008, , 2008, 5249.
[5] T. Tsuda, H. Murayama, K. Kitamura, N. Inadama, T. Yamaya, E. Yoshida, F. Nishikido, M. Hamamoto, H. Kawai, Y. Ono, IEEE Trans. Nucl. Sci. NS53 (2006) 35.
[6] Y. Shao, S.R. Cherry, S. Siegel, R.W. Silverman, IEEE Trans. Nucl. Sci. NS43 (1996) 1938.
[7] M. Rafecas, G. Boning, B.J. Pichler, E. Lorenz, M. Schwaiger, S.I. Ziegler, Phys. Med. Biol. 48 (2003) 821.
[8] G. Pratx, C.S. Levin, IEEE NSS-MIC 2007 2007 (2007) 2660.
[9] K.M. Champley, T.K. Lewellen, L.R. MacDonald, R.S. Miyaoka, P.E. Kinahan, Phys. Med. Biol. 54 (2009) 6369.
[10] A.A. Wagadarikar, A. Ivan, S. Dolinsky, D.L. McDaniel, IEEE Trans. Nucl. Sci. NS61 (2014) 121.
[11] T. Yamaya, T. Mitsuhashi, T. Matsumoto, N. Inadama, F. Nishikido, E. Yoshida, H. Murayama, H. Kawai, M. Suga, M. Watanabe, Phys. Med. Biol. 56 (2011) 6793.
[12] E. Yoshida, Y. Hirano, H. Tashima, N. Inadama, F. Nishikido, T. Moriya, T. Omura, M. Watanabe, H. Murayama, T. Yamaya, IEEE Trans. Nucl. Sci. NS60 (2013) 3172.
[13] S. Jan, G. Santin, D. Strul, S. Staelens, K. Assié, D. Autret, S. Avner, R. Barbier, M. Bardiès, P.M. Bloomfield, D. Brasse, V. Breton, P. Bruyndonckx, I. Buvat, A.F. Chatziioannou, Y. Choi, Y.H. Chung, C. Comtat, D. Donnarieix, L. Ferrer, S.J. Glick, C.J. Groiselle, D. Guez, P.F. Honore, S. Kerhoas-Cavata, A.S. Kirov, V. Kohli, M. Koole, M. Krieguer, D.J.J. van der Laan, F. Lamare, G. Largeron, C. Lartizien, D. Lazaro, M.C. Maas, L. Maigne, F. Mayet, F. Melot, C. Merheb, E. Pennacchio, J. Perez, U. Pietrzyk, F.R. Rannou, M. Rey, D.R. Schaart, C.R. Schmidtlein, L. Simon, T.Y. Song, J.-M. Vieira, D. Visvikis, R. Van de Walle, E. Wieërs, C. Morel, Phys. Med. Biol. 49 (2004) 4543.
[14] S. Jan, D. Benoit, E. Becheva, T. Carlier, F. Cassol, P. Descourt, T. Frisson, L. Grevillot, L. Guigues, L. Maigne, C. Morel, Y. Perrot, N. Rehfeld, D. Sarrut, D.R. Schaart, S. Stute, U. Pietrzyk, D. Visvikis, N. Zahra, I. Buvat, Phys. Med. Biol. 56 (2011) 881.
[15] K. Kamada, T. Yanagida, J. Pejchal, M. Nikl, T. Endo, K. Tsutsumi, Y. Fujimoto, A. Fukabori, A. Yoshikawa, IEEE Trans. Nucl. Sci. NS59 (2012) 2112.
[16] J. Iwanowska, L. Swiderski, T. Szczesniak, P. Sibczynski, M. Moszynski, M. Grodzicka, K. Kamada, K. Tsutsumi, Y. Usuki, T. Yanagida, A. Yoshikawa, Nucl. Instrum. Methods Phys. Res., Sect. A 712 (2013) 34.